Clays and Clay Minerals, Vol. 63, No. 5, 351–367, 2015.

THE STRUCTURE AND THERMOCHEMISTRY OF THREE Fe-Mg CHLORITES

STEPHEN AJA[1,*], OLADIPO OMOTOSO[2], CHRISTIAN BERTOLDI[3], EDGAR DACHS[3], AND ARTUR BENISEK[3]

[1] Department of Earth and Environmental Sciences, Brooklyn College of the City University of New York (CUNY), 2900 Bedford Avenue, Brooklyn, NY 11210-2889, USA

[2] Suncor Energy Inc. 150 6th Avenue SW Calgary, Alberta, T23 3P3, Canada

[3] Department of Materials Research and Physics, Mineralogy Division, University of Salzburg, Hellbrunner Str. 34, A-5020 Salzburg, Austria

Abstract—Chlorites are petrogenetically important minerals, exercise controls on petroleum reservoir qualities, are common in alteration zones during hydrothermal ore mineralization, and may form during carbon sequestration in sedimentary formations. Chlorite thermochemistry and structure have been investigated, in the present study, to facilitate an improved understanding of chlorite equilibria.

Three natural II*b* chlorites were studied by powder diffraction and calorimetric methods (low-temperature relaxation calorimetry using a Physical Properties Measurement System [PPMS] and differential scanning calorimetry [DSC]). The samples include a low-Fe clinochlore [Mg-Chl] and two Fe-rich chlorites from Windsor [Fe-Chl(W)] and Michigan [Fe-Chl(M)]. The structure of each chlorite was refined in the ideal *C*2/*m* symmetry using Rietveld techniques. Lattice parameters for the Windsor chlorite are a = 5.3786(6) Å, b = 9.3176(9) Å, c = 14.2187(6) Å, β = 96.98(10)º. The Michigan chlorite returned a = 5.3897(3) Å, b = 9.3300(3) Å, c = 14.2376(2) Å, β = 97.043(5)º whereas the low-Fe clinochlore yielded a = 5.3301(3) Å, b = 9.2231(8) Å, c = 14.2912(4) Å, β = 97.03(10)º.

Heat capacities (C_p) for the three natural chlorites were measured using both PPMS (2−303 K) and DSC (282−564 K). Employing a combination of Debye-Einstein-Schottky functions, the lattice dynamics component of the C_p at lower temperature was evaluated allowing a separation of the magnetic spin ordering component of C_p from the lattice vibrational part. For Mg-Chl, Fe-Chl(W), and Fe-Chl(M), the polynomials defining the temperature dependencies of the heat capacities between 280 and 570 K are:

$C_p = 1185.44(\pm68.93) - 9753.21(\pm2186.85)T^{-0.5} - 1.9094(\pm1.0288)\cdot10^7T^{-2} + 3.3013(\pm1.5363)\cdot10^9T^{-3}$

$C_p = 1006.06(\pm48.46) - 4134.83\ (\pm1515.16)T^{-0.5} - 40.0949(\pm6.9413)\cdot10^6T^{-2} + 5.9386(\pm1.0287)\cdot10^9T^{-3}$

and

$C_p = 1268.60(\pm67.16) - 11983.09(\pm2107.07)T^{-0.5} - 7.6037(\pm9.6417)\cdot10^6T^{-2} + 1.5398(\pm1.4187)\cdot10^9T^{-3}$,

respectively.

Standard state molar thermodynamic functions, C_P, S_T, $(H_T-H_0)/T$, and Φ were evaluated for the samples. $S_{298.15}$ for Fe-Chl(W), Mg-Chl, and Fe-Chl(M) were found to be 499.14 ± 3.40, 437.81 ± 3.00 and 515.06 ± 3.60 J mol^{-1}K^{-1}, respectively, whereas S^o for Fe-Chl(W) and Mg-Chl were determined to be 578.24 ± 3.76 and 503.21 ± 3.60 J mol^{-1}K^{-1}, respectively; these values emphasize that configurational entropy effects are consequential for chlorite thermochemistry.

Key Words—Calorimetric Entropy, Chlorite, Configurational Entropy, Excess Entropy, Heat Capacity, Magnetic Ordering, Rietveld Refinement, Ternary Chlorite Solid Solutions.

INTRODUCTION

The structure and thermochemistry of chlorites have continued to be of research interest to the geochemical community. Part of this interest stems from the wide variety of geologic environments in which chlorite is found (in low- to medium-grade regional metamorphic rocks, in pegmatites and fissure veins, and in hydrothermal alteration zones surrounding ore bodies: Rose and Burt, 1979; Guilbert and Park, Jr., 1986; De Haller and Fontboté, 2009). Chlorites are also common in siliciclastic petroleum reservoirs where their occurrence as pore-lining grain coatings leads to the preservation of anomalously high porosity and permeability (Berger *et al.*, 2009; Gould *et al.*, 2010). Interest in the stability of chlorites in low-temperature hydrothermal environments has also stemmed from the need for a better understanding of the geochemical consequences of carbon sequestration by injection of CO_2 into sedimentary formations (Haszeldine *et al.*, 2005; Lu *et al.*, 2012) and from the possible roles of chlorite−carbonate equilibria in generating over-pressures in sedimentary basins (Smith and Ehrenberg, 1989; Hutcheon, 1990).

Recent experimental investigations into the stability of chlorites under low-temperature hydrothermal conditions have included determination of equilibrium and/or kinetic constraints on chlorite solubility (Kittrick, 1982; Aja and Small, 1999; Aja and Dyar, 2002; Brandt *et al.*, 2003; Lowson *et al.*, 2005, 2007; Smith *et al.*, 2013; Black and Haese, 2014) and on calorimetric measurements (Hemingway *et al.*, 1984; Bertoldi *et al.*, 2001,

* E-mail address of corresponding author:
suaja@brooklyn.cuny.edu
DOI: 10.1346/CCMN.2015.0630502

2007; Gailhanou *et al.*, 2009). Calorimetric data, in conjunction with data from phase equilibrium experiments, typically provide the basis for retrieving standard-state thermodynamic properties of endmember chlorites (*e.g.* Holland and Powell, 1998; Grevel *et al.*, 2005; Holland and Powell, 2011).

Henderson *et al.* (1983) measured the heat content of a natural chromian clinochlore (X_{Fe} = 0.04) by low-temperature adiabatic calorimetry (low-TAC) and differential scanning calorimetry (DSC); the measurements of Henderson *et al.* (1983) provided the basis for the C_p polynomial of clinochlore in the Berman (1988) data set. Hemingway *et al.* (1984) measured heat capacity (low-TAC and DSC) for a clinochlore (X_{Fe} = 0.18) and a chamosite (X_{Fe} = 0.76) and reported calorimetric entropies of 431.7±5.0 J $mol^{-1}K^{-1}$ and 495.7±10.0 J mol^{-1} K^{-1} for the clinochlore and chamosite, respectively. Saccocia and Seyfried (1993) attempted to resolve discrepancies in the standard-state thermodynamic properties of endmember chamosite; in their study, they employed heat capacity predicted using the estimation algorithm of Berman and Brown (1985), and calorimetric entropy of chamosite computed using the oxide summation approach of Holland *et al.* (1998). Bertoldi *et al.* (2001) published heat capacities of two natural chlorites (X_{Fe} = 0.89 and X_{Fe} = 0.11) based on DSC measurement whereas Bertoldi *et al.* (2007) studied the heat capacities of four additional natural Fe-Mg chlorites (X_{Fe} between 0.052 and 0.885) using relaxation calorimetry; those authors determined the calorimetric standard entropy for endmember clinochlore and endmember chamosite to be 425.6±0.4 J $mol^{-1}K^{-1}$ and 505.1±0.2 J mol^{-1} K^{-1}, respectively. Gailhanou *et al.* (2009) measured the heat capacity of The Clay Minerals Society (CMS) Special Clay CCa-2, using low-TAC and DSC and reported calorimetric standard entropy of 469.4±2.9 J mol^{-1} K^{-1} for the sample. In the chlorites studied by Bertoldi *et al.* (2007) excess heat capacities, arising from magnetic ordering, were evaluated graphically whereas Gailhanou *et al.* (2009) employed a corresponding states approach (*cf.* Robie *et al.*, 1982) in their analyses. In none of these previous calorimetric investigations, however, were the configurational entropies of the individual chlorites determined.

For the most part, these prior studies either examined chlorite behaviors in hydrothermal solutions or measured thermodynamic properties of the chlorites using calorimetric techniques. Although solubility techniques provide a means of assessing directly the relative stability of minerals under hydrothermal conditions, they are of limited utility in yielding the fundamental thermochemical properties of the solid materials studied (Aja, 2002). On the other hand, the prediction of hydrothermal equilibria of complex phyllosilicates under low-temperature conditions using calorimetrically derived free energies of formation often lacks the desired resolution. In the present contribution, heat capacity and crystallographic data are reported for some natural chlorites previously investigated by solution equilibration techniques.

MATERIALS AND METHODS

Three natural chlorites (Figure 1) including a low-Fe clinochlore, a chlorite from Windsor, Quebec (hitherto Windsor chamosite) and a chamosite from Michigan, USA, were investigated in previous solution-equilibration techniques studies (Aja and Dyar, 2002). The Windsor sample was donated by the Canadian Museum of Nature (Ref. No. CMNMC 1796) and was described as minute granular dark green crystals consisting of microscopic vermiform aggregates of chamosite plates. The low-Fe clinochlore (Aja and Small, 1999) samples

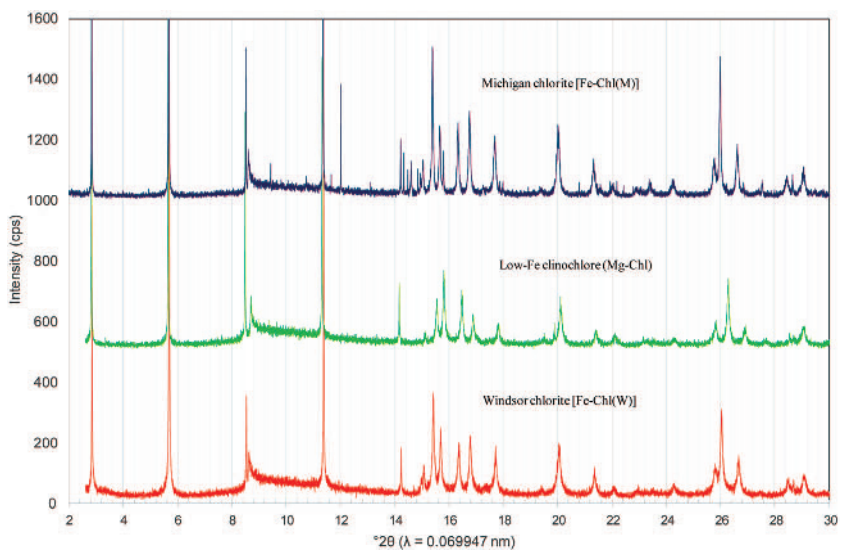

Figure 1. XRD profiles of the three chlorites used in the present study.

https://doi.org/10.1346/CCMN.2015.0630502 Published online by Cambridge University Press

were received as large, well crystallized plates. The Michigan chamosite was received as a massive, well indurated sample. The structural formulae of the Windsor chlorite, the low-Fe clinochlore, and the Michigan chlorite were heretofore reported as $(Fe^{3+}_{0.60}Fe^{2+}_{5.43}Mg_{2.30}Al_{2.98}Mn_{0.05}Ca_{0.03}Zn_{0.01}\square_{0.60})(Si_{5.63}Al_{2.37})O_{20}(OH)_{16}$, $(Al_{2.33}Fe^{2+}_{1.00}Fe^{3+}_{0.14}Ca_{0.02}Mn_{0.01}Ni_{0.02}Cr_{0.01}Mg_{8.40}\square_{0.07})(Si_{5.66}Al_{2.34})O_{20}(OH)_{16}$, and $(Al_{1.94}Ti_{0.28}Fe^{2+}_{6.16}Fe^{3+}_{0.56}Mn_{0.05}Mg_{2.05}Ca_{0.31}P_{0.19}V_{0.01}\square_{0.46})(Si_{5.26}Al_{2.74})O_{20}(OH)_{16}$ (Aja and Dyar, 2002). In what follows, the Windsor chlorite, low-Fe clinochlore, and Michigan chlorite are designated as Fe-Chl(W), Mg-Chl, and Fe-Chl(M), respectively.

For this re-investigation, the elemental compositions of the samples of the low-Fe clinochlore and the Windsor chlorite were re-determined using electron probe microanalysis (EPMA) (JEOL JXA-8900R, Tokyo, Japan). The major elements were determined using a JEOL JXA-8900R (Tokyo, Japan) microprobe at the University of Innsbruck, Institute for Geoscience, with 15 keV accelerating voltage, 20 nA probe current, and a beam size of 5 μm. Natural mineral standards from the Smithsonian Institution's National Museum of Natural History (Jarosewich *et al.*, 1980) were used as calibration standards. Matrix correction was performed with the JEOL implementation of Paul Carpenter (version 3.50) of the *CITZAF* software (Armstrong, 1995), which uses the $\phi(\rho z)$ algorithm of Armstrong (1982) for the absorption correction. The water contents of the chlorite samples were determined after thermal dehydration (1300ºC) using Karl-Fischer titration (KFT) at the University of Hannover's Institute for Mineralogy. A plan of the apparatus used in this study and a detailed description of the analytical procedures were given by Behrens and Stuke (2003).

Powder X-ray diffraction

For analyses by powder diffraction techniques, all the samples were wet milled to <5 μm with methanol in a micronizing mill. The slurry was allowed to evaporate at 60ºC. The dry powder was then mixed with plastic balls and sieved through a 400-mesh screen to produce near-spherical aggregates. Samples were mounted in 0.3 mm glass capillaries. Powder diffraction data were collected at the Advanced Photon Source (APS) at the Argonne National Laboratory (Chicago, Illinois, USA); the experiment was conducted at the high-resolution powder diffraction beamline 33-BM-C at λ = 0.69947 Å, between 2.6 and 40º2θ (15.4 and 1.02 Å), and a step size of 0.003º2θ. The primary beam was collimated to a 3 mm × 3 mm beam. A post-sample crystal analyser and a scintillation detector ensured a high-resolution set-up. The X-ray diffraction data were analysed using *TOPAS* Rietveld refinement software. The chlorite structure, in all three samples, was refined in the monoclinic II*b*-2 (*C*2/*m*) spacegroups (Brown and Bailey, 1962; Joswig and Fuess, 1990).

Low-temperature calorimetry

The heat-capacity option of the PPMS, produced by Quantum Design®, is based on the principles of relaxation calorimetry and allows the measurement of C_p on mg-sized samples. The PPMS measurements were performed at the Division for Material Science, University of Salzburg, and were repeated three times at each temperature step for 60 temperature set points between 2 K (Fe-rich chlorites) or 5 K (Mg-rich chlorite) and 300 K using a logarithmic spacing. The natural chlorite aggregates were first dried at 200ºC in a DSC device to expel adsorbed water and then wrapped in thin Al foil and pressed to a ~0.5 mm thick pellet for PPMS measurement; experimental details on the PPMS measurements have previously been reported by Dachs and Bertoldi (2005).

Differential scanning calorimetry

The heat capacities of the three chlorite samples between 282 and 764 K were measured with a Perkin Elmer Diamond DSC; details of the DSC experimental techniques have been published previously (Bertoldi *et al.*, 2001; Benisek *et al.*, 2009; Dachs and Benisek, 2011; Dachs *et al.*, 2012a, 2012b). Only the DSC data up to 564 K were used in generating C_p polynomials describing the temperature dependence of the data inasmuch as signs of chlorite decomposition were discernible above 564 K.

RESULTS

Elemental chemical composition

The bulk chemical compositions of the Windsor chlorite [Fe-Chl(W)] and the low-Fe clinochlore [Mg-Chl] samples, obtained from EPMA (Table 1), show that Na_2O, K_2O, CaO, and TiO_2 were below the detection limit of the electron microprobe; analytical uncertainties in computed atomic site occupancies are also reported (Table 1). The resulting structural formulae for the Windsor chlorite and low-Fe clinochlore are $(Al_{2.96}Fe^{3+}_{0.66}Fe^{2+}_{5.46}Mg_{2.38}Mn_{0.052}Zn_{0.014}\square_{0.474})(Si_{5.24}Al_{2.76})O_{20}(OH)_{16}$ and $(Al_{2.64}Cr^{3+}_{0.006}Fe^{3+}_{0.12}Fe^{2+}_{0.98}Mg_{7.94}Ni_{0.018}\square_{0.296})(Si_{5.72}Al_{2.28})O_{20}(OH)_{16}$, respectively ($Fe^{3+}$ was calculated from the Mössbauer spectroscopic results of Aja and Dyar, 2002). Some differences are apparent in the oxide compositions of the chlorites determined by EPMA (present study) and those determined by X-ray fluorescence spectroscopy (Aja and Dyar, 2002); in general, these compositions fall within the range of analytical uncertainty in terms of mole compositions. For instance, EPMA data yield a mole fraction of Fe in the octahedral site of 0.714±0.070 for the Windsor chlorite whereas the XRF data return a value of 0.719. Although the mole site occupancies obtained by the two analyses are identical, the elemental populations none-

https://doi.org/10.1346/CCMN.2015.0630502 Published online by Cambridge University Press

Table 1. EPMA-based composition of chlorite samples [Fe-Chl(W) and Mg-Chl].

	Fe-Chl(W) [1]n = 49	Mg-Chl n = 42
SiO_2	[2]24.13[3](49)	30.08(42)
Al_2O_3	22.45(61)	22.03(50)
Cr_2O_3	[4]u.d.l.	0.04(02)
[5]Fe_2O_3	4.09(06)	0.87(03)
[5]FeO	30.06(42)	6.18(22)
MgO	7.37(25)	28.06(53)
MnO	0.29(03)	u.d.l.
NiO	u.d.l.	0.12(01)
ZnO	0.09(04)	u.d.l.
[6]H_2O	11.10(08)	12.66(09)
Total	99.57	100.05
[7]FeO_{tot}	33.74(48)	6.96(25)
[8]$Fe^{3+}/\Sigma Fe$	0.109	0.112
Si	2.62(05)	2.86(05)
Al^{IV}	1.38(05)	1.14(05)
Al^{VI}	1.48(03)	1.32(02)
Cr^{3+}	u.d.l.	0.003(01)
Fe^{3+}	0.33(01)	0.06(01)
Fe^{2+}	2.73(04)	0.49(02)
Mg	1.19(03)	3.97(05)
Mn	0.026(03)	u.d.l.
Ni	u.d.l.	0.009(02)
Zn	0.007(04)	u.d.l.
S[VI]	5.77(03)	5.86(03)
(OH)	8.03(07)	8.02(06)
[9]X_{Fe}	0.714(07)	0.122(04)
[10]M	648.630	571.110
[11]m	18.62	19.12

Note that atomic site occupancies for chlorites are reported in this table on a half-cell basis $[O_{10}(OH)_8]$. In the text structural formulae are also denoted on a full-cell basis $[O_{20}(OH)_{16}]$.
[1]n: number of point analyses
[2] measured with EPMA, University of Innsbruck, Institute for Mineralogy
[3] ( ) numbers in parentheses are the standard deviations (1σ) and refer to the last digits
[4] u.d.l. = under detection limit
[5] Fe_2O_3 and FeO calculated from Mössbauer spectroscopy (Aja and Dyar, 2002)
[6] measured with Karl-Fischer-Titration, University of Hannover, Institute for Mineralogy
[7] FeO_{tot} derived from electron microprobe analysis
[8] $Fe^{3+}/\Sigma Fe$ derived from Mössbauer spectroscopy (Aja and Dyar, 2002)
[9] X_{Fe} = Fe/(Fe+Mn+Zn+Mg).
[10] M = mole weight (g/mol).
[11] m = sample weight (mg).

theless differ and may be consequential for retrieval of extensive thermodynamic properties. Hence, the analytical data obtained in the present study are preferred to those from previous analyses given that the water content of the chlorites was determined explicitly using Karl-Fischer titration techniques.

Rietveld analysis

Rietveld refinement was conducted in the ideal $C2/m$ space group using the structures proposed by Brown and Bailey (1962) as starting models with the octahedral cations distributed as indicated by the chemical analysis. A two-coefficient polynomial and a broadened cristobalite phase were used to model the background and the amorphous glass capillary. The two-dimensional diffraction bands were modeled using a symmetry-constrained anisotropic broadening function. In addition to refining the lattice parameters, the atomic positions and cation distribution in the octahedral sheets are refined with the cation–oxygen bond distance constrained to ~5% of the ideal bond distance. Oxygen–cation–oxygen bond angles were also constrained to within 5%. No ordering of silicon or aluminum was assumed in the tetrahedral sites $T1$ and $T2$. Both cations were distributed equally between the two sites according to the chemical analysis data. The cation in the $M4$ site was constrained to aluminum and excess aluminum allocated to $M3$. The scattering contrast between Fe and Mg (and Al) enabled a stable refinement of the cation distribution in $M1$, $M2$, and $M3$. Mg^{2+}, Al^{3+}, and Si^{4+} have essentially the same scattering factors and could not be differentiated by X-ray data. Preferred orientation, displacement parameters, and hydrogen positions were not refined. The presence of semi-random stacking is manifested in the slowly decaying intensity bands in the region between 8.6 and 9°2θ (Figure 1); this region is populated by hkl bands with $k \neq 3$. Diffraction profiles of the refined structures are provided in the supplementary appendix of this article submitted to the Editor in Chief and deposited at www.clays.org/journal/JournalDeposits.html.

Atomic site parameters and the resulting crystallographic data obtained from Rietveld refinement procedures are summarized in Tables 2 and 3, respectively. Within the resolution of the data collected, the Windsor chlorite and the low-Fe clinochlore are single phases, whereas ilmenite, quartz, and fluoroapatite peaks are prominent in the Michigan chlorite sample; these impurities have been estimated at 2.8%, 2.3%, and 2.2% for the ilmenite, quartz, and fluoroapatite, respectively.

Low-temperature and differential scanning calorimetry

The raw data for the heat capacities of the chlorites [Fe-Chl(W), Mg-Chl, Fe-Chl(M)], measured by PPMS under low-temperature conditions and by DSC above room temperature (Figure 2), are provided in the supplementary appendix. An excellent agreement exists between both calorimetric methods in the overlapping region around ambient temperature (Figure 2a,b,c); in the case of Fe-Chl(W) and Fe-Chl(M), PPMS measured heat capacity values are 0.2% and 0.6%, respectively, larger than DSC-measured heat capacity at 298 K. For sample Mg-Chl, the agreement is still good (PPMS-measured C_p is 1.3% larger than DSC-measured C_p).

https://doi.org/10.1346/CCMN.2015.0630502 Published online by Cambridge University Press

Table 2a. Refined atomic positions for low-Fe clinochlore (Mg-Chl).

Site		Atom	Multiplicity	*x*	y	z	Occupancy	β_{iso}
Mg1	M1	Mg^{2+}	2	0	0	0	0.810(11)	1
Fe1		Fe^{2+}	2	0	0	0	0.190(11)	1
Mg2	M2	Mg^{2+}	4	0	0.33222(13)	0	0.9631(59)	1
Fe2		Fe^{2+}	4	0	0.33222(13)	0	0.0369(59)	1
Mg3	M3	Mg^{2+}	4	0	0.16512(17)	0.5	0.6168(81)	1
Fe3		Fe^{2+}	4	0	0.16512(17)	0.5	0.1260(25)	1
Fe3		Fe^{3+}	4	0	0.16512(17)	0.5	0.03	1
Al3		Al^{3+}	4	0	0.16512(17)	0.5	0.1600(52)	1
Al4	M4	Al^{3+}	2	0	0.5	0.5	1	1
Si1	T1	Si^{4+}	8	0.22867(22)	0.167380(90)	0.191452(63)	0.715	1
Al1	T2	Al^{3+}	8	0.22867(22)	0.167380(90)	0.191452(63)	0.285	1
O1		O^{2-}	8	0.19159(33)	0.167380(90)	0.078300(79)	1	1
O2		O^{2-}	4	0.21404(36)	0	0.233263(69)	1	1
O3		O^{2-}	8	0.51089(60)	0.23697(20)	0.233263(69)	1	1
OH1		OH^{-}	4	0.19241(43)	0.5	0.07044(15)	1	1
OH2		OH^{-}	4	0.11877(95)	0	0.43078(19)	1	1
OH3		OH^{-}	8	0.13750(32)	0.34466(18)	0.428290(97)	1	1

Table 2b. Refined atomic site positions for the Windsor chlorite [Fe-Chl(W)].

Site		Atom	Multiplicity	*x*	y	z	Occupancy	β_{iso}
Fe1	M1	Fe^{2+}	2	0	0	0	0.72	1
Mg1	M1	Mg^{2+}	2	0	0	0	0.28	1
Mg2	M2	Mg^{2+}	4	0	0.3333(11)	0	0.28	1
Fe2		Fe^{2+}	4	0	0.3333(11)	0	0.72	1
Mg3	M3	Mg^{2+}	4	0	0.1666(13)	0.5	0.155	1
Fe3		Fe^{2+}	4	0	0.1666(07)	0.5	0.44	1
Fe3		Fe^{3+}	4	0	0.1666(07)	0.5	0.165	1
Al1		Al^{3+}	4	0	0.1666(13)	0.5	0.24	1
Al2	M4	Al^{3+}	2	0	0.5	0.5	1	1
Si1	T1	Si^{4+}	8	0.2310(32)	0.1666(13)	0.1920(05)	0.655	1
Al3	T2	Al^{3+}	8	0.2310(32)	0.1666(13)	0.1920(05)	0.345	1
O1		O^{2-}	4	0.1910(56)	0.1666(07)	0.0720(20)	1	1
O2		O^{2-}	4	0.2450(65)	0	0.2330(20)	1	1
O3		O^{2-}	8	0.4950(42)	0.2500(17)	0.2330(11)	1	1
OH1		OH^{-}	8	0.1910(57)	0.5	0.0720(10)	1	1
OH2		OH^{-}	4	0.1440(55)	0	0.4330(19)	1	1
OH3		OH^{-}	8	0.1440(58)	0.3333(21)	0.4330(12)	1	1

Table 3. Crystallographic data derived from Rietveld refinement.

	Fe-Chl(W)	Mg-Chl	Fe-Chl(M)
Space group	*C*2/*m*	*C*2/*m*	*C*2/*m*
a	5.3786(6)	5.3301(3)	5.3897(3)
b	9.3176(9)	9.2231(8)	9.3300(3)
c	14.2187(6)	14.2912(4)	14.2376(2)
α	90.0	90.0	90.0
β	96.98(10)	97.03(7)	97.043(5)
γ	90.0	90.0	90.0
Volume ($Å^3$)	707.25(5)	697.03(6)	710.55(4)
R_{wp}	26.5	18.49	23.21
R_{exp}	14.5	15.76	16.14
χ^2	3.3	1.7	2.1
Minimum *d*–*A*	1.09	1.09	1.09

https://doi.org/10.1346/CCMN.2015.0630502 Published online by Cambridge University Press

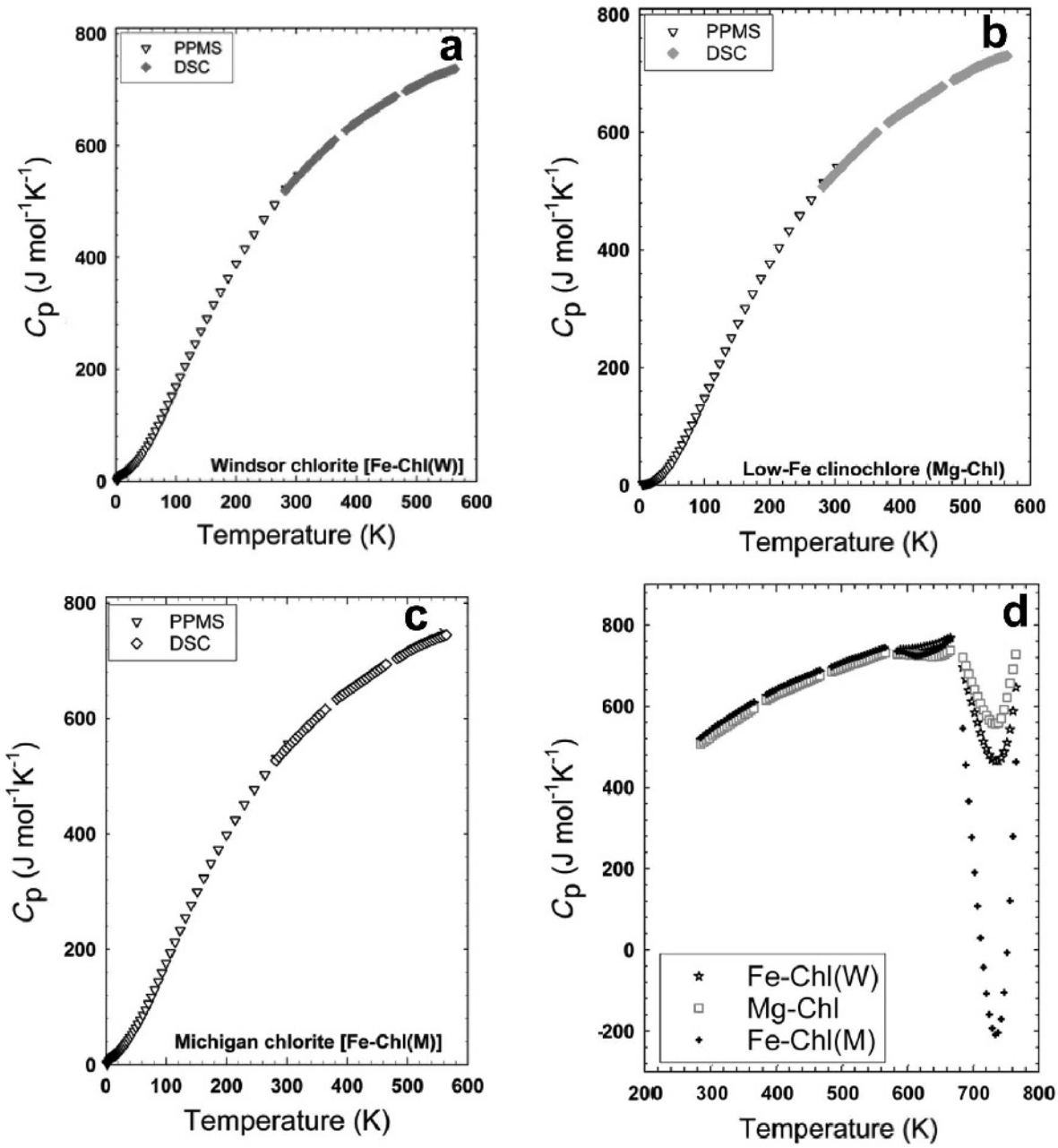

Figure 2. Molar heat capacities of Windsor chlorite [Fe-Chl(W)], low-Fe clinochlore (Mg-Chl), and Michigan chlorite [Fe-Chl(M)]; heat capacities below ambient temperatures were measured by PPMS whereas measurements above room temperature were obtained by DSC. The DSC data in parts a, b, and c represent the mean of three individual runs; in part d, individual DSC measurements up to 764 K are shown for the three chlorites and they show the breakdown of the chlorite samples at ~600 K and above.

Heat capacity measured by DSC indicates chlorite decomposition at temperatures of ~600 K and above for the three chlorites (Figure 2d). For the Michigan sample [Fe-Chl(M)], however, the DSC data suggest an exothermic reaction during the decomposition which may very well have been triggered by the minor extraneous phases in the sample. Hence, to retrieve standard-state thermodynamic properties for the chlorites, only C_p data up to 564 K were used.

The low-temperature segment (0−50 K) of the heat-capacity data (Figure 3) exhibit prominent C_p anomalies at temperatures of <20 K for Fe-Chl(W) and Fe-Chl(M), whereas for the low-Fe clinochlore the anomaly is more subdued. These anomalies result from the contributions of magnetic ordering to the heat capacities (Gopal, 1966; Bertoldi *et al.*, 2007; Gailhanou *et al.*, 2009), and quantifying the magnitudes of these excess heat capacities therefore serves important heuristic purposes.

https://doi.org/10.1346/CCMN.2015.0630502 Published online by Cambridge University Press

An evaluation of the calorimetric entropy function shows that at temperatures of >~20 K, the temperature dependence of the calorimetric entropy function approximates a well behaved function (*cf.* Figures 2, 3). But at temperatures of <20 K, an anomalous hump is superimposed on the entropy curve. Moreover, the height of the anomaly for the Fe-rich samples is more than triple the height of the anomaly for the low-Fe clinochlore, and at temperatures of 200 K and above, the difference in the temperature dependence of the entropy function decreases suggesting the dominance of lattice vibrations at these somewhat higher temperatures. Thus, these low-temperature calorimetric measurements accessed the contributions of magnetic ordering and the magnitude of the magnetic ordering (C_{mag}) can be determined if the vibrational (lattice) part of heat capacity (C_{vib}) is quantified.

Using the PPMS data for temperatures above the magnetic anomalies (>35 K for Fe-CHl(W) and Fe-Chl(M), and >22 K for Mg-Chl), the lattice dynamic part of the heat capacity was retrieved by fitting the equation (Boerio-Goates *et al.*, 2002);

$$C_p = 3R(mD(\Theta_D) + nE(\Theta_E) + sS(\Theta_S)) \quad (1)$$

where the Debye, Einstein, and Schottky functions are represented by $D(\Theta_D)$, $E(\Theta_E)$, and $S(\Theta_S)$, respectively; m, n, s, Θ_D, Θ_E, Θ_S are adjustable fit parameters and R is the universal gas constant.

The Debye [$D(\Theta_D)$], Einstein [$E(\Theta_E)$], and Schottky [$S(\Theta_S)$] functions are defined as follows:

$$D(\Theta_D) = 3\left(\frac{T}{\Theta_D}\right)^3 \int_0^{\frac{\Theta_D}{T}} \frac{x^4 e^x}{(e^x-1)^2} dx \quad (2)$$

$$E(\Theta_E) = \frac{\left(\frac{\Theta_E}{T}\right)^2 e^{\frac{\Theta_E}{T}}}{\left(e^{\frac{\Theta_E}{T}}-1\right)^2} \quad (3)$$

$$S(\Theta_S) = \frac{\left(\frac{\Theta_S}{T}\right)^2 e^{\frac{\Theta_S}{T}}}{\left(1+e^{\frac{\Theta_S}{T}}\right)^2} \quad (4)$$

The successful application of equation 1 to model heat-capacity data requires that the C_P data are truncated into two temperature sections (*cf.* Boerio-Goates *et al.*, 2002; Dachs *et al.*, 2010) with each temperature region being fitted independently (see Table 4 for the resulting fit coefficients and the corresponding temperature ranges). Having determined the lattice dynamics part of the heat capacity (C_{vib}) thus, the magnetic heat contribution was determined by difference, *i.e.*

$$C_{mag} = C_{p,measured} - C_{vib} \quad (5)$$

C_{mag} values (Figure 4) at the lowest temperatures (*i.e.* on the low-temperature flank of the observed excess heat capacity) were obtained by extrapolation. The two Fe-rich chlorites [Fe-Chl(W), Fe-Chl(M)] exhibit nearly identical

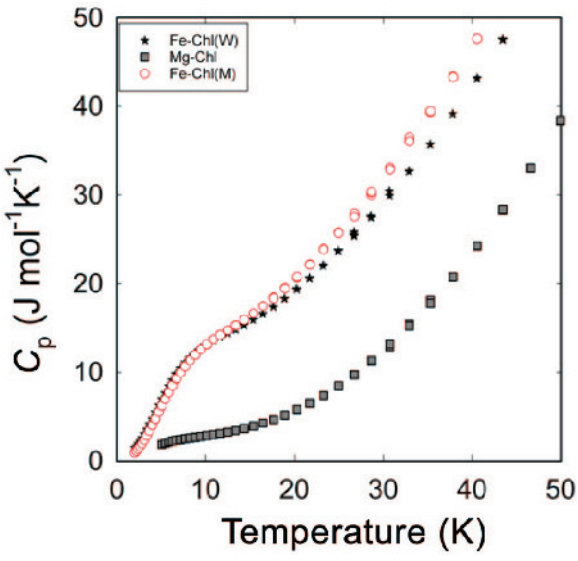

Figure 3. Temperature dependence of measured heat capacities for the three chlorites under very low temperatures (PPMS data). The Fe-rich chlorites, Windsor chlorite [Fe-Chl(W)], and Michigan chlorite [Fe-Chl(M)] show an anomaly (excess heat capacity) under 20 K attributable to magnetic ordering whereas the low-Fe clinochlore (Mg-Chl) has a much less pronounced magnetic ordering.

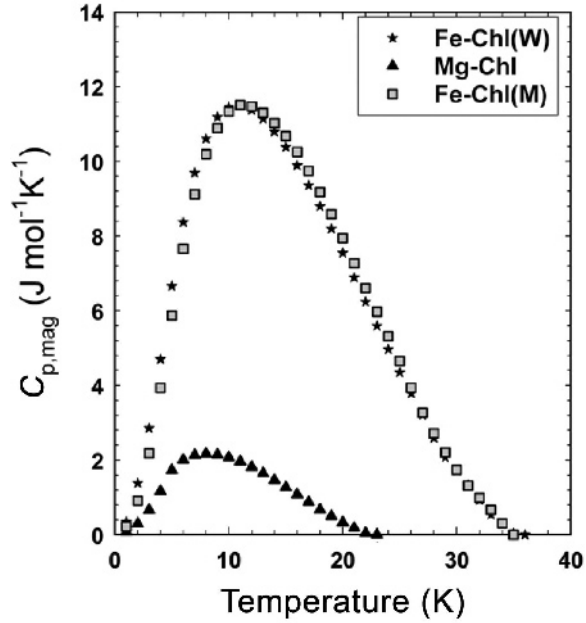

Figure 4. Contributions of magnetic ordering (C_{mag}) to the heat capacity of the chlorites as a function of temperature; at temperatures lower than experimental C_p data [2(5) K], C_{mag} was extrapolated by fitting the data to a function of the form $C_{mag} = A \cdot T^2 + B \cdot T^3 \exp(-D/T)$.

https://doi.org/10.1346/CCMN.2015.0630502 Published online by Cambridge University Press

Table 4. Fit parameters for Debye-Einstein-Schottky lattice vibrational C_p (equation 1).

	Fe-Chl(W)	Mg-Chl	Fe-Chl(M)
Lower temperatures			
m (mol)	3.2202	1.1159	3.7373
Θ_D (K)	157.0876	139.9123	161.9635
n (mol)	12.4886	7.1191	13.2015
Θ_E (K)	395.5302	285.5187	412.1115
ns (mol)	0.0000	0.0000	0.0000
Θ_S (K)	0.0000	0.0000	0.0000
Switching temperature (K)	79.7700	57.0418	88.2575
Higher temperatures			
m (mol)	18.8603	18.8935	19.3876
Θ_D (K)	539.9697	589.2643	541.8855
n (mol)	14.5646	12.8494	13.6331
Θ_E (K)	1071.4041	999.4216	1048.1393
ns (mol)	16.5855	1.8573	29.8067
Θ_S (K)	39.8496	173.9910	32.8361

magnetic ordering behaviors in terms of the shape of the profile and the peak temperature (11 K) of magnetic ordering. On the other hand, the peak magnetic ordering for the low-Fe clinochlore (Mg-Chl) occurs at a lower temperature (8 K), is less pronounced, and the profile shape is more asymmetric, suggesting that the ordering is quenched more gradually. The standard molar thermodynamic functions [C_P, S_T, $(H_T-H_0)/T$, and Φ] of the three chlorites calculated from modeled C_{vib} and C_{mag} behavior at selected temperatures (Table 5) assume no contribution from configurational entropy.

The C_p data obtained by DSC (282−564 K) and the uppermost PPMS data around ambient temperature were fit to a C_p polynomial of the form (Berman and Brown, 1985),

$$Cp = a + bT^{-0.5} + cT^{-2} + dT^{-3} \quad (6)$$

For all three chlorites, these model C_p polynomials (Table 6, Figure 5) reproduce the experimental data, in the temperature range 280−570 K, within 1 standard deviation (1σ) confidence interval.

DISCUSSION

Compositional variation of studied chlorites

The samples used in the present investigation may be described as a ferroan clinochlore [Mg-Chl] and magnesian chamosites [Fe-Chl(W), Fe-Chl(M)] (*cf.* Bailey, 1980) but to maintain consistency with nomenclature used in recent investigations and to underscore the great variety of these natural chlorites, the classification scheme of Foster (1962) has been used to describe the chlorite minerals. The low-Fe clinochlore (Mg-Chl) plots in the clinochlore field (Figure 6) whereas the Windsor and Michigan chlorites plot in the ripidolite field. In addition, virtually all Fe-rich natural chlorites used in recent invesigations plot in the ripidolite field (Figure 6) rather than in the chamosite field. Furthermore, samples of The CMS Special Clay (CCa-2) used in various studies may be described as several different chlorite minerals though this is not evident in some literature citations; in fact, Post and Plummer (1972) characterized this reference chlorite

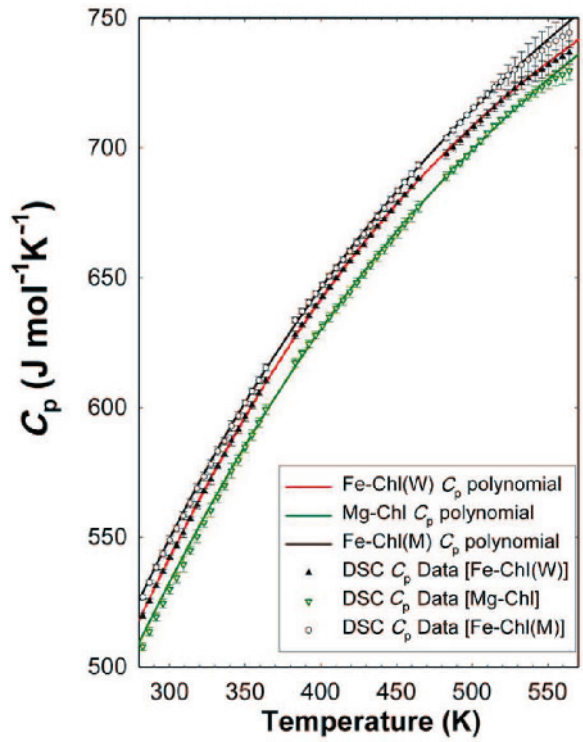

Figure 5. Correlation of fitted C_p polynomials (*cf.* Berman and Brown, 1985) with measured heat capacity data (DSC and uppermost ambient PPMS) for the three chlorites; the error bars show experimental errors at 1 standard deviation confidence interval.

https://doi.org/10.1346/CCMN.2015.0630502 Published online by Cambridge University Press

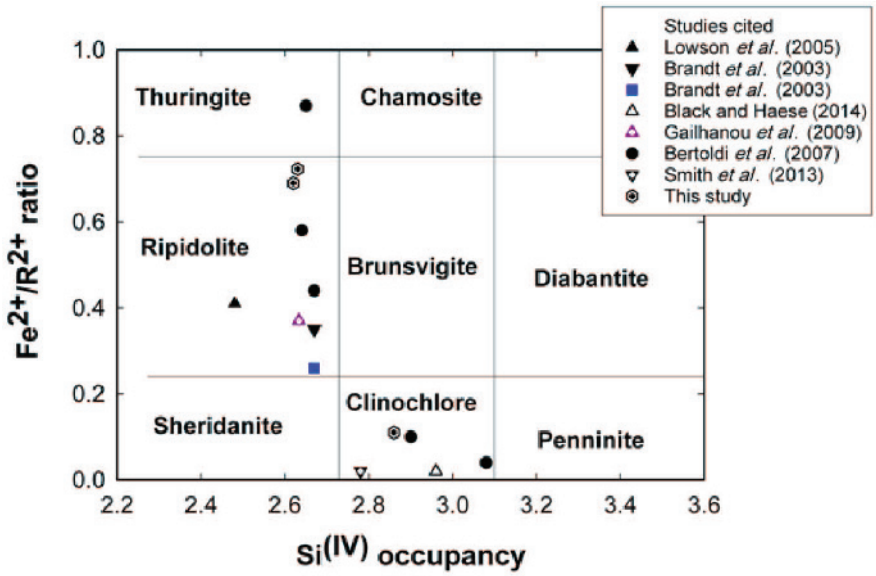

Figure 6. The compositions of natural chlorites, used in recent experimental investigations, projected onto the chemographic coordinates of Foster (1962); the mineralogical variations of The Clay Minerals Society Special Clay (CCa-2) utilized in recent studies is highlighted using triangles. The studies cited are previous calorimetric studies (Bertoldi *et al.*, 2007; Gailhanou *et al.*, 2009) and dissolution kinetics investigations (Brandt *et al.*, 2003; Lowson *et al.*, 2005; Smith *et al.*, 2013; Black and Haese, 2014).

sample as being made up of penninite, clinochlore, sheridanite, and ripidolite. Furthermore, none of the chlorites investigated have compositions that lie along the binary clinochlore $[(Mg_5Al)(AlSi_3)O_{10}(OH)_8]$–chamosite $[(Fe_5Al)(AlSi_3)O_{10}(OH)_8]$ join. Rather, they display varying degrees of Tschermak substitution away from the join, *i.e.* the following substitution:

$$Al^{IV} + Al^{VI} \rightleftharpoons Si^{IV} + R^{VI}$$

where R is Mg^{2+} or Fe^{2+}.

The effects of the Tschermak compositional vector along the binary join are usually considered in modeling physicochemical properties determined for natural chlorite samples (*e.g.* Bertoldi *et al.*, 2007) although there is, as yet, no standard way of doing this.

The presence of variable amounts of iron in chlorites (Figure 6) implies that magnetic ordering is consequential in chlorite thermochemistry but it is questionable whether their effects have been accounted for sufficiently in previous compilations of standard-state thermodynamic properties for end-member chlorites based on calorimetry of natural chlorites. The magnetic susceptibilities of different natural chlorites peak at different low-temperature conditions (Ballet *et al.*, 1985) and the peak of magnetic susceptibility, which coincides with the onset of magnetic ordering, will thus vary for different chlorites given the variable range of Fe contents. C_{mag} peaks at ~11 K [Fe-Chl(W) and Fe-Chl(M)] and 8 K (Mg-Chl) (Figure 4); by contrast, however, some literature data (*e.g.* Townsend *et al.*, 1986) suggest that magnetic ordering occurs at temperatures of <7 K.

Structural chemistry of chlorites

Chlorites are phyllosilicates in which adjacent 2:1 layers are linked by an octahedral sheet. The most common chlorites are tri-trioctahedral (or trioctahedral) in which all three cation positions in the octahedral sheet of the 2:1 layer (often referred to as the talc layer) are occupied and the interlayer is also trioctahedral with a brucite sheet in which all three octahedral positions are occupied. The structural formulae for the brucite sheet and the 2:1 talc layer are $R^{2+}_{6-y_1-z_1}R^{3+}_{y_2}\square_{z_1})(OH)_{12}$ and $R^{2+}_{6-y_2-z_2}R^{3+}_{y_2}\square_{z_2})(Si^{4+}_{4-k}R^{3+}_{k})_2O_{20}(OH)_4$, respectively; hence the general structural formula for chlorites, $R^{2+}_{6-y-z}R^{3+}_{y}\square_{z})_2(Si_{4-k}R^{3+}_{k})_2O_{20}(OH)_{16}$ (Zazzi *et al.*, 2006). The total octahedral vacancy (z) is the sum of the vacancies in both octahedral sheets (z_1 and z_2) and y is the sum of y_1 and y_2. The talc layer is often negatively charged from Al^{3+} substitution for Si^{4+} in the tetrahedral sheet. The negative charge is balanced by a positively charged brucite sheet in which Al^{3+} substitutes for Mg^{2+}. In the tetrahedral sheet of the talc layer, the trivalent cation R^{3+}_k is usually aluminum and confers on the sheet a negative charge equal to $2 \times k$; this negative charge is balanced by positive charges from the substitution in the octahedral sheets of trivalent cations for divalent cations. In chamosite and clinochlore, Fe^{2+} and Mg^{2+} are the dominant divalent cations in the octahedral sheets. The trivalent cation is often Al^{3+} or Fe^{3+}. Two cation sites exist in each octahedral sheet and they are often represented by $M1$ and $M2$ in the talc octahedral sheet and $M3$ and $M4$ in the brucite sheet. $M1$ and $M4$ are centrosymmetric and less distorted than $M2$ and $M3$. The

https://doi.org/10.1346/CCMN.2015.0630502 Published online by Cambridge University Press

Table 5a. Smoothed molar thermodynamic functions for Fe-Chl(W).

T (K)	C_p J mol^{-1}K^{-1}	S_T J mol^{-1}K^{-1}	$(H_T-H_0)/T$ J mol^{-1}K^{-1}	Φ J mol^{-1}K^{-1}
1	0.34682	0.17313	0.11547	0.057652
2	1.3938	0.69471	0.46351	0.2312
3	2.8951	1.5351	1.0161	0.51895
4	4.8039	2.6239	1.7198	0.90413
5	6.8630	3.9144	2.5400	1.3743
6	8.7209	5.3361	3.4210	1.9150
7	10.243	6.7994	4.2912	2.5082
8	11.436	8.2488	5.1133	3.1355
9	12.361	9.6522	5.8700	3.7821
10	13.073	10.993	6.5558	4.4367
11	13.648	12.266	7.1752	5.0911
12	14.157	13.476	7.7361	5.7399
13	14.662	14.629	8.2496	6.3796
14	15.170	15.735	8.7259	7.0086
15	15.726	16.800	9.1737	7.6261
20	19.173	21.766	11.217	10.549
25	23.775	26.518	13.250	13.268
30	29.244	31.321	15.446	15.876
35	35.351	36.280	17.846	18.434
40	42.832	41.488	20.501	20.987
45	50.428	46.969	23.401	23.567
50	58.499	52.694	26.502	26.192
60	76.953	64.94	33.327	31.614
70	98.457	78.385	41.064	37.320
80	121.73	93.042	49.685	43.357
90	144.62	108.68	58.941	49.739
100	169.01	125.17	68.722	56.450
110	193.74	142.44	78.964	63.477
120	218.18	160.35	89.551	70.800
130	242.03	178.76	100.37	78.394
140	265.15	197.55	111.32	86.232
150	287.54	216.61	122.32	94.287
160	309.20	235.86	133.33	102.53
170	330.17	255.24	144.29	110.95
180	350.45	274.69	155.19	119.50
190	370.06	294.16	165.98	128.18
200	389.01	313.63	176.66	136.97
210	407.29	333.06	187.21	145.84
220	424.90	352.41	197.62	154.79
230	441.84	371.68	207.87	163.80
240	458.11	390.83	217.96	172.87
250	473.71	409.85	227.88	181.96
260	488.65	428.72	237.63	191.09
270	502.93	447.43	247.19	200.24
280	516.57	465.97	256.57	209.40
290	529.59	484.33	265.76	218.56
298.15	539.62	499.14	273.11	226.03

Table 5b. Smoothed molar thermodynamic functions for Mg-Chl.

T (K)	C_p J mol^{-1}K^{-1}	S_T J mol^{-1}K^{-1}	$(H_T - H_0)/T$ J mol^{-1}K^{-1}	Φ J mol^{-1}K^{-1}
1	0.074392	0.03706	0.024731	0.012329
2	0.30074	0.14931	0.099717	0.049591
3	0.68366	0.33832	0.22614	0.11218
4	1.2204	0.60511	0.40466	0.20045
5	1.8278	0.9434	0.62922	0.31419
6	2.1743	1.31	0.86027	0.44971
7	2.4016	1.6649	1.0667	0.5982
8	2.5749	1.997	1.2445	0.7525
9	2.7158	2.3086	1.4003	0.90828
10	2.8629	2.6024	1.5392	1.0631
11	3.0065	2.8819	1.6660	1.2159
12	3.1698	3.1504	1.7844	1.3660
13	3.3586	3.4114	1.8981	1.5133
14	3.5765	3.6681	2.0101	1.6581
15	3.8323	3.9234	2.1228	1.8006
20	5.6724	5.2549	2.7601	2.4948
25	8.7007	6.8171	3.6196	3.1975
30	12.606	8.7381	4.7822	3.9559
35	17.400	11.028	6.2295	4.7980
40	23.371	13.727	7.9861	5.7409
45	30.537	16.883	10.083	6.7992
50	38.685	20.514	12.529	7.9851
60	56.859	29.138	18.370	10.768
70	77.475	39.423	25.315	14.108
80	100.09	51.225	33.230	17.995
90	124.13	64.390	41.984	22.407
100	148.97	78.749	51.436	27.314
110	174.11	94.126	61.445	32.682
120	199.15	110.35	71.879	38.473
130	223.87	127.27	82.622	44.649
140	248.08	144.75	93.579	51.171
150	271.69	162.68	104.67	58.005
160	294.63	180.95	115.83	65.117
170	316.83	199.48	127.00	72.474
180	338.25	218.2	138.15	80.049
190	358.88	237.04	149.23	87.815
200	378.67	255.96	160.21	95.75
210	397.62	274.89	171.06	103.83
220	415.73	293.81	181.78	112.04
230	433.00	312.68	192.33	120.35
240	449.43	331.45	202.70	128.75
250	465.06	350.12	212.89	137.24
260	479.89	368.65	222.87	145.78
270	493.96	387.03	232.65	154.38
280	507.29	405.24	242.23	163.01
290	519.92	423.26	251.59	171.67
298.15	529.71	437.81	259.06	178.75

Note: $\Phi = S_T - (H_T - H_0)/T$

concentration of aluminum in the brucite *M*4 site is common (Rule and Bailey, 1987; Welch et al.,1995; Zazzi *et al.*, 2006).

Chlorites, like most phyllosilicates, exhibit a semi-random stacking disorder whereby the hydrogen bond between the brucite interlayer and the talc 2:1 layers above and below the brucite sheet can assume, at random, any of three positions separated by $\pm b/3$ (Brown and Bailey, 1962; Rule and Bailey, 1987). The II*b* polytype is the most abundant chlorite polytype found in nature (Brown and Bailey, 1962); the II symbol represents one of two brucite sheet orientations (I and II) in which the slope of the brucite sheet is in a direction opposite to that of the talc octahedral sheet. The *b* symbol denotes the location of the hydrogen bond between the brucite hydroxyl and talc tetrahedral oxygen atoms such that brucite cations are not superimposed on

https://doi.org/10.1346/CCMN.2015.0630502 Published online by Cambridge University Press

Table 5c. Smoothed molar thermodynamic functions for Fe-Chl(M).

T (K)	C_p J mol^{-1}K^{-1}	S_T J mol^{-1}K^{-1}	$(H_T - H_0)/T$ J mol^{-1}K^{-1}	Φ J mol^{-1}K^{-1}
1	0.22181	0.11057	0.073769	0.036799
2	0.92025	0.44833	0.30009	0.14824
3	2.2233	1.0501	0.70921	0.34088
4	4.0409	1.9302	1.3077	0.62255
5	6.0781	3.0511	2.0583	0.99275
6	8.0316	4.3342	2.8932	1.441
7	9.705	5.7039	3.7523	1.9516
8	11.065	7.0917	4.5843	2.5074
9	12.139	8.4599	5.3668	3.0931
10	13.037	9.7861	6.09	3.696
11	13.781	11.065	6.7566	4.3086
12	14.416	12.292	7.3686	4.9231
13	15.037	13.471	7.935	5.5356
14	15.673	14.608	8.4649	6.1432
15	16.355	15.713	8.968	6.7445
20	20.431	20.947	11.3	9.6464
25	25.786	26.06	13.642	12.418
30	31.995	31.286	16.161	15.125
35	39.046	36.746	18.926	17.82
40	47.389	42.509	21.966	20.543
45	55.568	48.562	25.245	23.317
50	63.982	54.849	28.694	26.154
60	82.644	68.12	36.091	32.029
70	104.2	82.444	44.249	38.195
80	127.8	97.883	53.204	44.679
90	151.91	114.33	62.838	51.496
100	176.13	131.58	72.947	58.637
110	200.99	149.53	83.456	66.079
120	225.73	168.09	94.284	73.803
130	249.96	187.12	105.33	81.785
140	273.5	206.51	116.51	89.999
150	296.3	226.16	127.74	98.42
160	318.33	245.99	138.96	107.02
170	339.6	265.93	150.14	115.78
180	360.12	285.92	161.24	124.68
190	379.88	305.93	172.23	133.69
200	398.9	325.9	183.09	142.8
210	417.17	345.81	193.81	152
220	434.71	365.62	204.36	161.26
230	451.5	385.32	214.75	170.57
240	467.56	404.88	224.95	179.93
250	482.91	424.28	234.96	189.31
260	497.55	443.5	244.78	198.72
270	511.5	462.54	254.4	208.14
280	524.78	481.39	263.83	217.56
290	537.41	500.03	273.04	226.99
298.15	547.18	515.06	280.4	234.65

the adjacent talc tetrahedral cations. In the alternative *a* position, brucite cations are superimposed on talc tetrahedral cations causing increased cation–cation repulsion (Rule and Bailey, 1987). Both *a* and *b* orientations can adopt one of six positions with optimal hydrogen bonding between the brucite hydroxyls and the center of the hexagonal ring of the repeating talc tetrahedral sheet. Positions 1 and 2 lie on the mirror plane of the original talc and brucite stack and therefore have a greater symmetry than the other four positions which are offset from the mirror plane. Brown and Bailey (1962) noted that all chlorites with semi-random stacking sequence would have triclinic symmetry as a result of averaging the three random positions. In the II*b* polytype, two of these positions result in a triclinic symmetry for the chlorite layer, (*e.g.* II*b* – 4 (or 5), IIb – 6 (or 3)), and the third, II*b* – 2 (or 1) confers monoclinic symmetry. A consequence of this semi-random sequence is that only atoms that are spaced by $\pm b/3$ within each layer are periodic along the **c*** axis. All other atoms are aperiodic along **c*** and will cause diffuse $k \neq 3n$ reflections. Structure refinement using powder diffraction data of the II*b* polytype with semi-random disorder is often conducted in the $C\bar{1}$ space group because of the random stacking sequence and because the triclinic form is the most commonly observed in ordered chlorites. In C*2/m*, F(*hkl*) = F($h\bar{k}l$) and can be used to differentiate the monoclinic form from the triclinic form. The *hkl* and $h\bar{k}l$ reflections are, however, often unresolved in powder patterns.

In the three natural II*b* chlorites that were investigated, semi-random stacking of the adjacent talc layer precluded the differentiation of the II*b*-2 polytype from the II*b*-4 by powder diffraction. The ideal symmetry *C*2/*m* of the 1-layer chlorite was, therefore, used for Rietveld refinement. Although the diffraction data do not provide complete three-dimensional structural elucidations, the cation composition and location in the octahedral talc layer and brucite sheet were refineable with minimal constraints, as were the OH positions along the ~ $\pm b/3$ repeat distance. The 2-dimensional diffraction bands corresponding to $k \neq 3n$ peaks were modeled by a symmetry-constrained anisotropic broadening model.

The refined structural formulae of the chlorites are reported in the form $(M_1,M_2)(M_3,M_4)(T_1,T_2)O_{20}(OH)_{16}$; for the refinements, only the major cations were considered and atomic site occupancies were initially

Table 6. Coefficients for the heat capacity polynomial $Cp = a + bT^{-0.5} + cT^{-2} + dT^{-3}$.

Sample	a	b	$c \times 10^7$	$d \times 10^9$
Fe-ChI(W)	1006.06 ± 48.46	−4134.83 ± 1515.16	−4.0094 ± 0.6941	5.9386 ± 1.0287
Mg-Chl	1185.44 ± 68.93	−9753.21 ± 2186.85	−1.9094 ± 1.0288	3.3013 ± 1.5363
Fe-Chl (M)	1268.60 ± 67.16	−11983.09 ± 2107.07	−0.7603 ± 0.9641	1.5398 ± 1.4187

https://doi.org/10.1346/CCMN.2015.0630502 Published online by Cambridge University Press

constrained using the EPMA analyses (Table 1). The composition of the Windsor chlorite refined to $(Fe^{2+}_{4.32}Mg_{1.68})(Fe^{2+}_{1.76}Fe^{3+}_{0.66}Mg_{0.62}Al_{2.96})(Si_{5.16}Al_{2.84})O_{20}(OH)_{16}$ whereas for the low-Fe clinochlore, the refined structural composition is $(Mg_{5.47}Fe^{2+}_{0.53})(Al_{2.64}Mg_{2.47}Fe^{2+}_{0.50}Fe^{3+}_{0.12}\square_{0.27})(Si_{5.72}Al_{2.28})O_{20}(OH)_{16}$.

Despite the small *R* factors obtained for the refinements, tetrahedral atom positions other than those along the *z* axis cannot be determined uniquely from powder diffraction data due to the semi-random disorder observed for these minerals. The refined structural chemistry of the Michigan chlorite [Fe-Chl(M)] is not reported here because of imprecision in atomic occupancy caused by Fe contributed by the ilmenite impurity.

Entropy of the natural chlorites

Various entropies (Table 7) have been retrieved for the three chlorites from the calorimetric and structural data reported here.

Configurational entropy. Configurational entropies were calculated for the chlorites using the expression

$$S_{conf} = -R\Sigma_j m_j \Sigma_i X_{i,j} \ln X_{i,j} \quad (7)$$

R is the gas constant, m_j is the crystallographic multiplicity of atomic site *j* divided by the number of formula units per cell, and $X_{i,j}$ is the atomic fraction of species *i* on site *j*.

Configurational entropies thus deduced for the Mg-Chl and Fe-Chl(W) are 65.4±2.0, and 79.1±0.7 J mol^{-1} K^{-}, respectively (Table 7). As is to be expected, these chemical entropy effects are greater than the configurational entropy of 37.4 J mol^{-1}K^{-1} expected for stoichiometric phases such as endmember clinochlore $[(Mg_2Mg_4)(Mg_4Al_2)(Si_6Al_2)O_{20}(OH)_{16}]$ (or chamosite) the chemical configurational entropy of which derives from occupancy and disorder of the tetrahedral sites. These configurational entropies have comparable magnitudes, however, with the configurational entropy of 68.62 J mol^{-1} K^{-1} reported by Ulbrich and Waldbaum (1976) for a ripidolite of composition $Mg_{1.3}Fe_{3.4}Al_{1.3}(Si_{2.7}Al_{1.3})O_{10}(OH)_8$. On the other hand, they also reported much lower configurational entropies for two Mg-corundophilites. For the sample $Mg_6(Si_{2.5}Al_{1.5})O_{10}(OH)_8$, they reported a value of 22.1 J mol^{-1}K^{-1} (based on a random mixing of Si and Al over four tetrahedral sites) whereas they reported a value of 18.7 J mol^{-1}K^{-1} for the second sample, $Mg_4Al_2(Si_2Al_2)O_{10}(OH)_8$ (assuming the site preferences: X^{T1}_{Si} = 0.25, X^{T1}_{Al} = 0.75 and *vice versa* for *T*2). Clearly, the configurational entropy effects are somewhat consequential for chlorites although in most previous calorimetric studies (*cf.* Hemingway *et al.*, 1984; Bertoldi *et al.*, 2007; Gailhanou *et al.*, 2009), the lack of the pertinent structural data apparently precluded evaluation of these entropy effects.

Third law entropy. By definition, the third law entropy may be given as the sum of the calorimetric and residual entropies (Ulbrich and Waldbaum, 1976); *i.e.*

$$S^o = \int_0^{298.15}(C_p/T)dT + \Delta S_p + \Delta S_{conf} \quad (8)$$

In this study, it is presumed that the residual entropy is approximated by the configurational entropy owing to site mixing (ΔS_{conf}) and that the associated phase-change entropies (ΔS_p) derive primarily from magnetic spin ordering; other types of phase changes are not known to occur for chlorites under the conditions of the experiment. Inasmuch as the very low temperatures of the calorimetric measurements assured access to the contribution of magnetic ordering to the heat capacities and the detailed crystallographic data allowed determination of the configurational entropies, the third law entropies could then be determined using equation 8 (see results in Table 7).

Table 7. Heat capacities at 298.15 K, standard state calorimetric ($S_{298.15}$), and third law (S^o) entropies (J mol^{-1}K^{-1}) for investigated chlorites.

	Fe-Chl(W)	Mg-Chl	Fe-Chl(M)
$C_{p,\ 298.15}$	539.62 ± 0.40	529.71 ± 0.30	547.18 ± 0.40
$S_{298.15}$	499.14 ± 3.40	437.81 ± 3.00	515.06 ± 3.60
S_{mag}	19.62	2.55	18.64
S_{vib}	479.52	435.26	496.42
S_{conf}	79.1 ± 1.60	65.4 ± 2.00	n.d.
S^o	578.24 ± 3.80	503.21 ± 3.60	n.d.
S^{ex}	28.3	10.1	40.5

S_{mag}, S_{vib}, and S_{conf} designate entropy due to magnetic ordering (or magnetic entropy), entropy contributed by lattice vibrations (or ideal vibrational entropy), and configurational entropy arising from distribution of atoms in the structure (or chemical entropy), respectively. S^{ex} is the excess entropy from mixing stoichiometric chlorite endmembers (amesite, chamosite, clinochlore); configurational entropy and third law entropy were not determined (n.d.) for Fe-Chl(M). S_i^o (J mol^{-1}K^{-1}) for amesite, chamosite, and clinochlore (390, 545, and 410.50, respectively) obtained from Holland and Powell (1998) were used to determine S^{ex} reported here.

https://doi.org/10.1346/CCMN.2015.0630502 Published online by Cambridge University Press

Implications for chlorite solid solution

Certain aspects of chlorite solid-solution behavior are highlighted by recent calorimetric data (Hemingway *et al.*, 1982; Bertoldi *et al.*, 2007; Gailhanou *et al.*, 2009; present study); the calorimetric entropies show a somewhat linear dependence on the mole fraction of Fe (Figure 7). Such a linear trend normally implies little or slightly positive excess vibrational entropy in the solid solutions. The ideal clinochlore–chamosite mixing line presumed using data from Holland and Powell (2011) is, however, offset from the observed linear trend by 14–25 J $mol^{-1}K^{-1}$ (Figure 7). By contrast, an ideal mixing line, presumed on the basis of the data set of Holland and Powell (1998), appears to fit the observed trend; this discrepancy between the two data sets may reflect assumptions inherent in their correlation algorithms and underscores the need for further refinement in the presumed standard state thermodynamic properties of the endmember phases.

Formulating a ternary solid-solution model for chlorites. Petrogenetic models of chlorite equilibria often utilize four or more endmember components including Mg-amesite [$(Mg_4Al_2)(Si_2Al_2)O_{10}(OH)_8$], chamosite [$(Fe_5Al)(Si_3Al)O_{10}(OH)_8$], clinochlore [$(Mg_5Al)(Si_3Al)O_{10}(OH)_8$], sudoite [$(Mg_2Al_3\square_1)(Si_3Al)O_{10}(OH)_8$], and Al-free chlorite [$Mg_6Si_4O_{10}(OH)_8$] (*cf.* Holland *et al.*, 1998; Lanari *et al.*, 2014). Given that none of the samples in this study has fully tetrasilicic occupancy, the Al-free chlorite may be excluded as an endmember. Secondly, sudoite may be excluded as an endmember inasmuch as its tetrahedral occupancy is same as that of chamosite and clinochlore; although this minimizes the contribution of octahedral vacancy, the latter constitutes <4% of octahedral site populations (see Table 1). The relevant endmembers are, therefore, presumed to be amesite, chamosite and clinochlore.

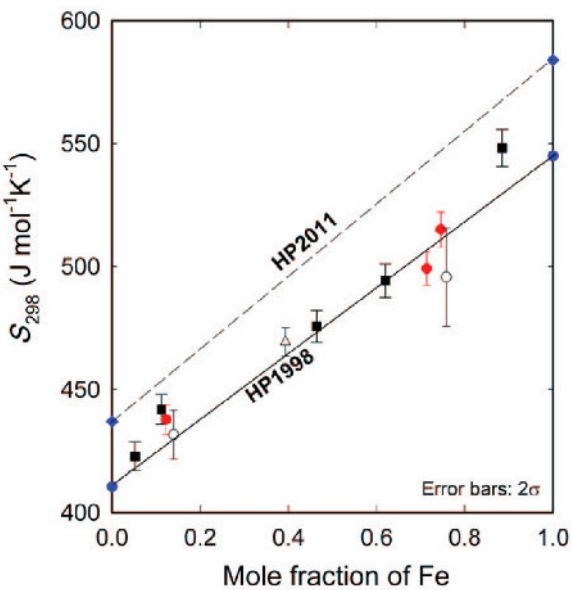

Figure 7. Variation of calorimetric entropies for some natural Fe-Mg chlorites at 298 K as a function of mole fraction of Fe (Fe^{2+}/R^{2+}). The solid circles, solid squares, open triangle, and open circles depict S_{298} values obtained from the present study, and from Bertoldi *et al.* (2007), Gailhanou *et al.* (2009), and Hemingway *et al.* (1984), respectively. The dashed and solid straight lines show the ideal mixing behavior between clinochlore and chamosite using S_{298} reported by Holland and Powell (2011) and Holland and Powell (1998), respectively.

Both chamosite and clinochlore have one Al in their tetrahedral sites whereas amesite has two. Tetrahedral aluminum (Al^{IV}) greater than one per half unit cell in natural aluminous chlorites, therefore, represents solid solution towards amesite away from the clinochlore–chamosite join. The mole fraction of amesite in the natural samples may then be set as the difference between the Al content of the natural sample and that of endmember clinochlore (or chamosite). In the present study, the mole components of the relevant endmembers are determined as shown below:

	Tetrahedral occupancy	$X_{amesite}$	X_{Fe}	$X_{chamosite}$	X_{clc}
Fe-Chl (W)	$(Si_{2.62}Al_{1.38})/O_{10}(OH)_8$	0.38	0.714	0.44	0.18
Mg-Chl	$(Si_{2.86}Al_{1.14})/O_{10}(OH)_8$	0.14	0.122	0.10	0.76
Fe-Chl (M)	$(Si_{2.63}Al_{1.37})/O_{10}(OH)_8$	0.37	0.746	0.47	0.16

The mole fraction of Fe, X_{Fe}, is obtained from chemical analyses of the samples (*cf.* Table 1). When projected onto the chamosite–clinochlore binary join, X_{Fe} is simply presumed to be the mole fraction of chamosite but in this ternary model,

$$X_{chamosite} = (X_{Fe})(1-X_{amesite})$$

and

$$X_{clc} = 1 - (X_{amesite} + X_{chamosite})$$

The ternary system clinochlore–chamosite–amesite thus provides a means to incorporate the Tschermak component into simplified models of chlorite equilibria. The compositions of the natural chlorites used in these calorimetric investigations (Hemingway *et al.*. 1984; Bertoldi *et al.*, 2007; Gailhanou *et al.*, 2009; present study) are depicted in this ternary system (Figure 8a).

The general applicability of this ternary model to natural chlorites has been demonstrated using compositions of chlorites initially reported by Foster (1962); 84% of these chlorite compositions fall within the amesite–chamosite–clinochlore solid solution (Figure 8b). For natural Fe-Mg chlorites with tetrahedral aluminum <1, the compositional variation can still be modeled in a ternary system. In this case, the Tschermak solid substitution is toward the chlorite endmember having tetrasilicic occupancy and thus the applicable endmembers will be chamosite, clinochlore, and Al-free chlorite (Figure 8c). These ternary systems may provide the basis for less complex thermodynamic models (cf. Lanari *et al.*, 2014) of chlorite geothermometry.

https://doi.org/10.1346/CCMN.2015.0630502 Published online by Cambridge University Press

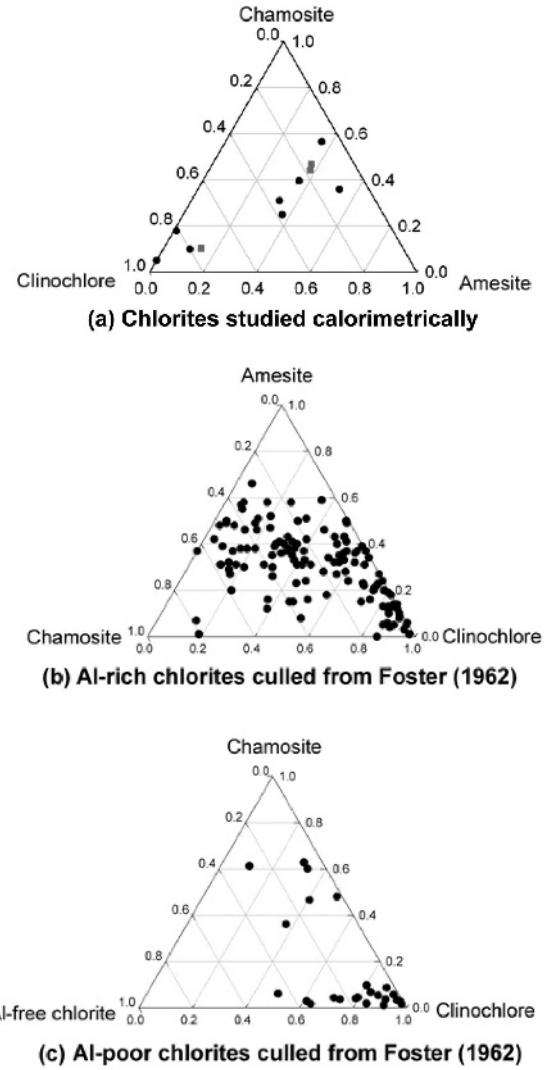

Figure 8. Compositional variation of natural chlorites in ternary compositional space: (a) variation of chlorite compositions utilized in recent calorimetric measurements in the amesite–chamosite–clinochlore system [solid squares (this study), solid circles (Hemingway *et al.*, 1984; Bertoldi *et al.*, 2007; Gailhanou *et al.*, 2009)]; (b) projection of compositions of Al-rich chlorites (from Foster, 1962) onto the amesite–chamosite–clinochlore space; (c) projection of compositions of Al-poor chlorites (from Foster, 1962) onto the Al-free chlorite–chamosite–clinochlore ternary compositional space.

Excess entropy of solid solutions. The excess entropy of mixing of the endmembers (amesite, clinochlore, chamosite) to yield solid solutions equivalent to the natural chlorites, without any explicit provision for substitutional ordering of the atoms, may be calculated using the general model (Anderson and Crerar, 1993; p. 377)

$$S^{ex} = S_{real} - S_{ideal} = S_{Chl,measured} - \left(\sum_i X_i S_i^o - R\sum_i X_i \ln X_i\right) \quad (9)$$

S_{real} is the calorimetric entropy (or $S_{Chl,measured}$), and S_i^o and X_i refer to the calorimetric entropy and mole fraction of the endmember components, respectively.

Equation 9 is applicable to both the binary (clinochlore–chamosite) and the ternary (amesite–chamosite–clinochlore) systems. In the binary system, the excess entropy of mixing appears sinusoidal (Figure 9a); the high-Mg samples show a positive deviation whereas the Fe-rich phases behave differently. Metal alloys may exhibit sinusoidal dependence of excess entropies on mole compositions (*e.g.* Lai and Yih, 1986) although this is not common for silicate solid solutions and perhaps underscores the fact that the chamosite–clinochlore system is, in fact, a pseudobinary system inasmuch as the mole fraction of iron is equated to the mole fraction of chamosite. By contrast, in the ternary system, the magnitudes of the excess entropies of mixing decrease with increasing mole fraction of clinochlore yielding a curvilinear dependence on mole compositions (Figure 9b); using S_{298} for endmember phases from Holland and Powell (1998) and Vidal *et al.* (2005) leads to significantly different excess entropies of mixing. The entropy of mixing also shows a correlation with molar volume (Figure 9c). Calorimetric entropies of these natural chlorites fall within and are bounded by the three linear entropy–volume correlations rather than along the chamosite–clinochlore join or chamosite–amesite join (Figure 9d). The curvilinear dependence probably then derives from pairwise interacting entropy–volume correlations of the constituent binaries of the ternary system. Excess vibrational entropies of solid solutions reflect differences between molar volumes and bulk moduli of limiting endmember phases (Benisek and Dachs, 2011, 2012) and thus the correlation with molar volumes shown herein suggests the applicability of such a model.

SUMMARY

The crystallographic and thermochemical properties of three natural non-stoichiometric chlorites [Fe-Chl(W), Mg-Chl, and Fe-Chl(M)] were investigated in the present study. X-ray diffraction data of the chlorites were refined in the ideal symmetry *C*2/*m* of the 1-layer chlorite using Rietveld techniques; the refinement yielded the cation composition and location in the octahedral talc and brucite sheets with minimal constraints as well as the OH positions along the ~±*b*/3 repeat distance. A comparative chemographic overview of chlorites used in recent studies indicates that chamosite, *sensu stricto*, has not featured in previous investigations.

Heat capacities for the chlorites were measured using both PPMS (2–303 K) and DSC (282–564 K); at 298.15 K, C_p was determined to be 539.62 ± 0.43, 529.71 ± 0.37, and 547.18 ± 0.44 J mol^{-1}K^{-1} for Fe-Chl(W), Mg-Chl, and Fe-Chl(M), respectively. For the three chlorite

https://doi.org/10.1346/CCMN.2015.0630502 Published online by Cambridge University Press

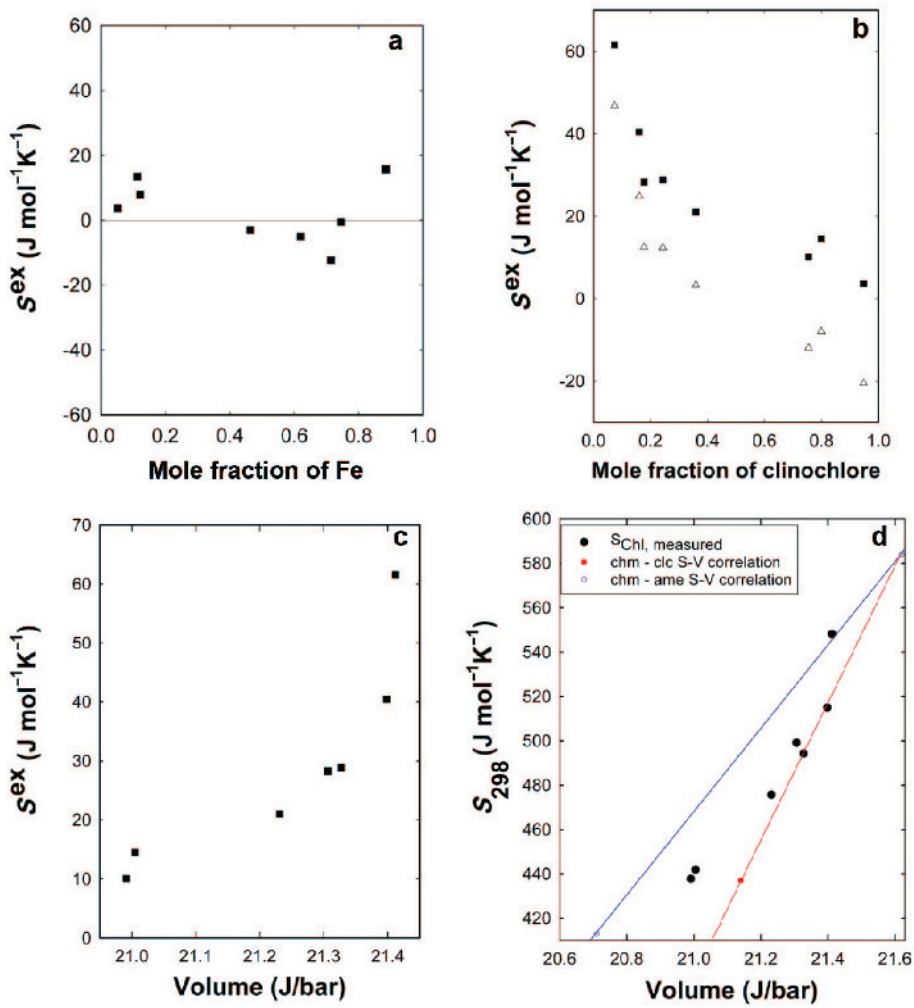

Figure 9. Excess entropy (S^{ex}) of chlorite solid solution from mixing molecular endmember components: (a) variation of S^{ex} for the pseudobinary chamosite–clinochlore with mole fraction of Fe; (b) variation of S^{ex} for the ternary system amesite–chamosite–clinochlore with mole fraction of clinochlore; (c) correlation of S^{ex} in the ternary system as a function of molar volumes of chlorites; (d) correlation of S_{298} (solid circles) of natural chlorites (present study, Bertoldi *et al.*, 2007) with molar volumes. Molar volumes were calculated from unit-cell volumes reported in Table 3 (present study) and by Lougear *et al.* (2000). Solid squares (■) indicate entropy of mixing calculated using entropy of endmembers from Holland and Powell (1998) whereas open triangles (Δ) indicate results using entropy of endmember phases from Vidal *et al.* (2005). The alternate choice of reference entropies yielded a difference of between 15 and 22 J mol^{-1}K^{-1}; for each reference database, the lowest entropy of mixing is found for the Mg-rich chlorites.

samples, S_{298} values were established as 499.14 ± 3.40, 437.81 ± 3.00, and 515.06 ± 3.60 J mol^{-1} K^{-1}, respectively. Calorimetric entropies for natural chlorites show an apparent linear dependence with mole fraction of Fe, although an ideal solid-solution model in the pseudobinary chamosite–clinochlore system cannot be presumed. In the ternary amesite–chamosite–clinochlore solid solution, the excess entropy of mixing of the chlorites displays a curvilinear pattern consistent with an entropy–volume correlation. The excess entropies of mixing stoichiometric chlorites to yield solid solutions equivalent to investigated natural chlorites (S^{ex}) have lower magnitudes than the excess entropy of multisite mixing (S_{conf}) for the same natural chlorite samples.

ACKNOWLEDGMENTS

Part of this study was supported by a grant from the Petroleum Research Fund administered by the American Chemical Society (ACS-PRF# 29930-AC2) and by the University Committee on Research Awards (PSC – CUNY: RF No. 6-66205, 6-667208) Program. Helpful review comments by Dr Velbel, Associate Editor Huertas, Dr Neuhoff and anonymous journal reviewers are gratefully acknowledged.

REFERENCES

Aja, S.U. (2002) The stability of Fe-Mg chlorites in hydrothermal solutions: II. Thermodynamic properties. *Clays and Clay Minerals*, **50**, 591–600.

https://doi.org/10.1346/CCMN.2015.0630502 Published online by Cambridge University Press

Aja, S.U. and Dyar, M.D. (2002) The stability of Fe-Mg chlorites in hydrothermal solutions I. Results of experimental investigations. *Applied Geochemistry*, **17**, 1219–1239.

Aja, S.U. and Small, J.S. (1999) The solubility of a low-Fe clinochlore between 25 and 175ºC and $P_v = P_{H2O}$. *European Journal of Mineralogy*, **11**, 829–842

Anderson, G.M. and Crerar, D.A. (1993) *Thermodynamics in Geochemistry: The Equilibrium Model*. Oxford University Press, Oxford, UK.

Armstrong, J.T. (1982) New ZAF and a-factor correction procedures for the quantitative analysis of individual microparticles. Pp. 175–180 in: *Microbeam Analysis* (K.F.J. Heinrich, editor). San Francisco Press, San Francisco, California, USA.

Armstrong, J.T. (1995) CITZAF: A package of correction programs for the quantitative electron microbeam X-ray analyses of thick polished materials, thin films and particles. *Microbeam Analyses*, **4**, 177–200.

Bailey, S.W. (1980) Summary of recommendations of AIPEA nomenclature committee on clay minerals. *American Mineralogist*, **65**, 1–7.

Ballet, O., Coey, J.M.D., and Burke, K.J. (1985) Magnetic properties of sheet silicates: 2:1:1 layer minerals. *Physics and Chemistry of Minerals*, **12**, 370–378.

Behrens, H. and Stuke, A. (2003) Quantification of H_2O contents in silicate glasses using IR spectroscopy – a calibration based on hydrous glasses analyzed by Karl-Fischer titration. *Glass Science and Technology*, **76**, 176–189.

Benisek, A. and Dachs, E. (2011) On the nature of the excess heat capacity of mixing. *Physics and Chemistry of Minerals*, **38**, 185–191.

Benisek, A. and Dachs, E. (2012) A relationship to estimate the excess entropy of mixing: Application in silicate solid solutions and binary alloys. *Journal of Alloys and Compounds*, **527**, 127–131.

Benisek, A., Dachs, E., and Kroll, H. (2009) Excess heat capacity and entropy of mixing in high structural state plagioclase. *American Mineralogist*, **94**, 1153–1161.

Berger, A., Gier, S., and Krois, P. (2009) Porosity – preserving chlorite cements in shallow-marine volcaniclastic sandstones: evidence from Cretaceous sandstones of the Sawan gas field, Pakistan. *American Association of Petroleum Geology Bulletin*, **93**, 595–615.

Berman, R.G. (1988) Internally consistent thermodynamic data for stoichiometric minerals in the system Na_2O-K_2O-CaO-MgO-FeO-Fe_2O_3-Al_2O_3-SiO_2-TiO_2-H_2O-CO_2. *Journal of Petrology*, **29**, 445–522.

Berman, R.G. and Brown, T.H. (1985) Heat capacity of minerals in the system Na_2O-K_2O-CaO-MgO-FeO-Fe_2O_3-Al_2O_3-SiO_2-TiO_2-H_2O-CO_2: representation, estimation, and high temperature extrapolation. *Contributions to Mineralogy and Petrology*, **89**, 168–183.

Bertoldi, C., Benisek, A., Čemic, L., and Dachs, E. (2001) The heat capacity of two natural chlorite group minerals derived from differential scanning calorimetry. *Physics and Chemistry of Minerals*, **28**, 332–336.

Bertoldi, C., Dachs, E., and Appel, P. (2007) Heat pulse calorimetry on natural chlorite-group minerals. *American Mineralogist*, **92**, 553–559.

Black, J.R. and Haese, R.R. (2014) Chlorite dissolution rates under CO_2 saturated conditions from 50 to 120ºC and 120 to 200 bar CO_2. *Geochimica et Cosmochimica Acta*, **125**, 225–240.

Boerio-Goates, J., Stevens, R., Hom, B.K., Woodfield, B.F., Piccione, P.M., Davis, M.E., and Navrotsky A. (2002) Heat capacities, third-law entropies and thermodynamic functions of SiO_2 molecular sieves from T = 0 K to 400 K. *Journal of Chemical Thermodynamics*, **34**, 205–227.

Brandt, F., Bosbach, D., Krawczyk-Bärsch, E., Arnold, T., and Bernhard, G. (2003) Chlorite dissolution in the acid pH-range: a combined microscopic and macroscopic approach. *Geochimica et Cosmochimica Acta*, **67**, 1451–1461.

Brown, B.E. and Bailey, S.W. (1962) Chlorite polytypism: I. Regular and semi-random one-layer structure. *American Mineralogist*, **47**, 819–850.

Dachs, E. and Benisek, A. (2011) A sample-saving method for heat capacity measurements on powders using relaxation calorimetry. *Cryogenics*, **51**, 460–464.

Dachs, E. and Bertoldi, C. (2005) Precision and accuracy of the heat-pulse calorimetric technique: Low-temperature heat capacities of milligram-sized synthetic mineral samples. *European Journal of Mineralogy*, **17**, 251–259.

Dachs, E., Harlov, D., and Benisek, A. (2010) Excess heat capacity and entropy of mixing along the chlorapatite–fluorapatite binary join. *Physics and Chemistry of Minerals*, **37**, 1–12.

Dachs, E., Geiger, C.A., Benisek, A., and Grevel, K.D. (2012a) Thermodynamic properties of grossular garnet: Heat capacity behavior, standard entropy and selected petrologic applications. *American Mineralogist*, **97**, 1299–1313.

Dachs, E., Geiger, C.A., and Benisek, A. (2012b) Almandine: Lattice and non-lattice heat capacity behavior and standard thermodynamic properties. *American Mineralogist*, **97**, 1171–1182.

De Haller, A. and Fontboté, L. (2009) The Raúl-Condenstable iron oxide copper-gold deposit, Central Coast of Peru: Ore and related hydrothermal alteration, sulfur isotopes, and thermodynamic constraints. *Economic Geology*, **104**, 365–384.

Foster, M.D. (1962) Interpretation of the composition and classification of chlorites. *Geological Survey Profesional Paper*, **414-A**, 1–33.

Gailhanou, H., Rogez, J., van Miltenburg, J.C., van Genderen, A.C.G., Greńche, J.M., Gilles, C., Jalabert, D., Michau, N., Gaucher, E.C., and Blanc, P. (2009) Thermodynamic properties of chlorite CCa-2. Heat capacities, heat contents and entropies. *Geochimica et Cosmochimica Acta*, **73**, 4738–4749.

Gopal, E.S.R. (1966) *Specific Heats at Low Temperatures.* Heywood Books, London.

Gould, K., Pe-piper, G., and Piper, D.J.W. (2010) Relationship of diagenetic chlorite rims to depositional facies in lower Cretaceous reservoir sandstones of the Scotian Basin. *Sedimentology*, **57**, 587–610.

Grevel, K.D., Kahl, W.A., Majzlan, J., Navrotsky, A., Lathe, C., and Flockenberg, T. (2005) Thermodynamic properties of magnesium chloritoid. *European Journal of Mineralogy*, **17**, 587–598.

Guilbert, J.M. and Park, Jr, C.F. (1986) *The Geology of Ore Deposits*. W. H. Freeman, New York.

Haszeldine, R.S., Quinn, O., England, G., Wilkinson, M., Shipton, Z.K., Evans, J.P., Heath, J., Crossey, L., Ballentine, C.J., and Graham, C.M. (2005) Natural geochemical analogues for carbon dioxide storage in deep geological porous reservoirs, a United Kingdom perspective. *Oil & Gas Science and Technology – Revue d'IFP Energies Nouvelle*, **60**, 33–49.

Hemingway, B.S., Kittrick, J.A., Grew, E.S., Nelen, J.A., and London, D. (1984) The heat capacity of osumilite from 298.15 to 1000 K, the thermodynamic properties of natural chlorites to 500 K, and the thermodynamic properties of petalite to 1800 K. *American Mineralogist*, **69**, 701–710.

Henderson, C.E., Essene, E.J., Anovitz, L.M., Westrum, E.F., Hemingway, B.S., and Bowman, J.R. (1983) Thermodynamic and phase equilibria of clinochlore, $(Mg_5Al)[Si_3AlO_{10}](OH)_8$. *Transactions of the American*

https://doi.org/10.1346/CCMN.2015.0630502 Published online by Cambridge University Press

Geophysical Union, **64**, 466.

Holland, T.J.B. and Powell, R. (1998) An internally consistent thermodynamic dataset for phases of petrological interest. *Journal of Metamorphic Geology*, **16**, 309–343.

Holland, T.J.B. and Powell, R. (2011) An improved and extended internally consistent thermodynamic dataset for phases of petrological interest, involving a new equation of state for solids. *Journal of Metamorphic Geology*, **29**, 333–383.

Holland, T.J.B., Baker, J., and Powell, R. (1998) Mixing properties and activity-composition relationships of chlorites in the system MgO-FeO-Al_2O_3-SiO_2-H_2O. *European Journal of Mineralogy*, **10**, 395–406.

Hutcheon, I. (1990) Clay–carbonate reactions in the Venture area, Scotian Shelf, Nova Scotia, Canada Pp. 199–212 in: *Fluid-Mineral Interactions: A tribute to H. P. Eugster* (R.J. Spencer and I.-M. Chou, editors). Special Publication, **2**, Geochemical Society, St. Louis, Missouri, USA.

Jarosewich, E., Nelen, J.A., and Norberg, J.A. (1980) Reference samples for electron microprobe analysis. *Geostandards Newsletters*, **4**, 43–47.

Joswig, W. and Fuess, H. (1990) Refinement of a one-layer triclinic chlorite. *Clays and Clay Minerals*, **38**, 216–218.

Kittrick, J.A. (1982) Solubility of two high-Mg and two high-Fe chlorites using multiple equilibria. *Clays and Clay Minerals*, **30**, 167–179.

Lai, S.K. and Yih, T.S. (1986) Excess entropy and resistivity of Mg-based alloys. *Physica*, **141B**, 191–198.

Lanari, P., Wagner, T., and Vidal, O. (2014) A thermodynamic model for di-trioctahedral chlorite from experimental and natural data in the system MgO-FeO-Al_2O_3-SiO_2-H_2O: applications to P-T sections and geothermometry. *Contributions to Mineralogy and Petrology*, **167**, 968–976.

Lougear, A., Grodzicki, M., Bertoldi, C., Trautwein, A.X., Steiner, K., and Amthauer, G. (2000) Mössbauer and molecular orbital study of chlorites. *Physics and Chemistry of Minerals*, **27**, 258–269.

Lowson, R.T., Comarmond, M.-C.J., Rajaratnam, G., and Brown, P. (2005) The kinetics of dissolution of chlorite as a function of pH and at 25ºC. *Geochimica et Cosmochimica Acta*, **69**, 1687–1699.

Lowson, R.T., Brown, P.L., Comarmond, M.-C.J., and Rajaratnam, G. (2007) The kinetics of chlorite dissolution. *Geochimica et Cosmochimica Acta*, **71**, 1431–1447.

Lu, J., Kharaka, Y.K., Thorsden, J.J., Horita, J., Karamalidis, A., Grifith, C., Hakala, J.A., Ambats, G., Cole, D.R., Phelps, T.J., Manning, M.A., Cook, P.J., and Hovorka, S.D. (2012) CO_2-rock-brine interactions in Lower Tuscaloosa Formation at Cranfield CO_2 sequestration site, Mississippi, USA. *Chemical Geology*, **291**, 269–277.

Post, J.L. and Plummer, C.C. (1972) The chlorite series of Flagstaff Hill Area, California: A preliminary investigation. *Clays and Clay Minerals*, **20**, 271–283.

Robie, R.A., Hemingway, B.S., and Takei, H. (1982) Heat capacities and entropies of Mg_2SiO_4, Mn_2SiO_4, and Co_2SiO_4 between 5 and 380 K. *American Mineralogist*, **67**, 470–482.

Rose, A.W. and Burt, D.M. (1979) Hydrothermal alteration. Pp. 173–235 in: *Geochemistry of Hydrothermal Ore Deposits* (H.L. Barnes, editor). Wiley-Interscience, New Jersey, USA.

Rule, A.C. and Bailey, S.W. (1987) Refinement of the crystal structure of a monoclinic ferroan clinochlore. *Clays and Clay Minerals*, **35**, 129–138.

Saccocia, P.J. and Seyfried, W.E. Jr. (1993) A resolution of discrepant thermodynamic properties for chamosite retrieved from experimental and empirical techniques. *American Mineralogist*, **78**, 607–611.

Smith, J.T. and Ehrenberg, S.N. (1989) Correlation of carbon dioxide abundance with temperature in clastic hydrocarbon reservoirs. *Marine and Petroleum Geology*, **6**, 129–135.

Smith, M.M., Wolery, T.J., and Carroll, S.A. (2013) Kinetics of chlorite dissolution at elevated temperatures and CO_2 conditions. *Chemical Geology*, **347**, 1–8.

Townsend, M.G., Longworth, G., and Kodama, H. (1986) Magnetic interaction at low temperature in chlorite and its products of oxidation: A Mössbauer investigation. *The Canadian Mineralogist*, **24**, 105–115.

Ulbrich, H.H. and Waldbaum, D.R. (1976) Structural and other contributions to the third-law entropies of silicates. *Geochimica et Cosmochimica Acta*, **40**, 1–24.

Vidal, O., Parra, T., and Vieillard, P. (2005) Thermodynamic properties of the Tschermak solid solution in Fe-chlorite: Application to natural examples and possible role of oxidation. *American Mineralogist*, **90**, 347–358.

Welch, M.D., Barris, J., and Klinowski, J. (1995) A multinuclear NMR study of clinochlore. *American Mineralogist*, **80**, 441–447.

Zazzi, A., Hirsch, T.K., Leonova, E., Kaikkonen, A., Grins, J., Annersten, H., and Eded, M. (2006) Structural investigations of natural and synthetic chlorite minerals by X-ray diffraction, Mössbauer spectroscopy and solid-state nuclear magnetic resonance. *Clays and Clay Minerals*, **54**, 252–265.

(*Received 19 October 2014; revised 27 October 2015; Ms. 926; AE: F. Javier Huertas*)